

Tuning the standard SCR reaction kinetics to model NO conversion in a diesel engine exhaust SCR catalyst system under steady state conditions in 1D and 3D geometries using ammonia gas as the reductant

Benjamin, S.F. , Gall, M. and Roberts, C.A.

Published version deposited in CURVE April 2013

Original citation & hyperlink:

Benjamin, S., Gall, M., and Roberts, C. (2012). *Tuning the standard SCR reaction kinetics to model NO conversion in a diesel engine exhaust SCR catalyst system under steady state conditions in 1D and 3D geometries using ammonia gas as the reductant*. SAE Technical Paper 2012-01-1636.

<http://dx.doi.org/10.4271/2012-01-1636>

Publisher statement: SAE paper 2012-01-1636 Copyright © 2012 SAE International. This paper is posted on this site with permission from SAE International. Further use or distribution of this paper is not permitted without permission from SAE.

Copyright © and Moral Rights are retained by the author(s) and/ or other copyright owners. A copy can be downloaded for personal non-commercial research or study, without prior permission or charge. This item cannot be reproduced or quoted extensively from without first obtaining permission in writing from the copyright holder(s). The content must not be changed in any way or sold commercially in any format or medium without the formal permission of the copyright holders.

CURVE is the Institutional Repository for Coventry University

<http://curve.coventry.ac.uk/open>

Tuning the Standard SCR Reaction Kinetics to Model NO Conversion in a Diesel Engine Exhaust SCR Catalyst System Under Steady State Conditions in 1D and 3D Geometries Using Ammonia Gas as the Reductant

2012-01-1636

Published
09/10/2012

S. F. Benjamin, M. Gall and C. A. Roberts
Coventry University, UK

Copyright © 2012 SAE International

doi:10.4271/2012-01-1636

ABSTRACT

Removal of NO_x from lean Diesel exhaust can be achieved by the use of selective catalytic reduction technology. The supplied reductant is often ammonia, either as urea or as ammonia gas released from a storage medium. Experiments have been carried out on an engine test rig run to steady state conditions using NO_x composed mainly of NO, with ammonia gas as the reductant. This was essentially a 1D study because a long 10 degree diffuser was used to provide uniform temperature and velocity profile to the SCR catalyst brick in the test exhaust system. Tuning of the standard reaction, the NO SCR reaction, in a kinetic scheme from the literature and adjustment of the ammonia adsorption kinetics achieved improved agreement between the measurements and CFD simulations. This was carried out for studies at exhaust gas temperatures between 200 and 300 °C. The effect of diffuser geometry upstream of the SCR catalyst on NO_x conversion was then investigated experimentally using a 180 degree sudden expansion as a 3D diffuser. These were also steady state studies with the exhaust NO_x composed mostly of NO. The SCR brick was short, 45 mm in length, to provide a rigorous test of the kinetics. Observed NO_x conversion profiles for ammonia supplied in quantities ranging from deficient to excess showed that the combined influence of temperature and velocity profiles upstream of the SCR was apparent in this 3D case. 2D axially symmetric CFD simulations have been carried out to model the 3D case and the predictions are discussed and compared with engine test data in this paper.

INTRODUCTION

Removal of NO_x from lean Diesel exhaust can be achieved by the use of selective catalytic reduction technology and this is one of the methods of choice to achieve the Euro 6 targets for passenger cars by 2014. The supplied reductant is often ammonia, supplied either as an aqueous urea spray or as ammonia gas released from a storage medium. Experiments have been carried out on an engine test rig run to steady state conditions using NO_x composed mainly of NO, with ammonia gas as the reductant. The engine was run without EGR so that significant and easily measurable levels of NO_x were produced. A series of experiments has been carried out aimed at providing a data set for validation of a CFD model. Initial experiments under 1D conditions have provided data that have enabled a kinetic scheme to be tested and modified. This data was obtained using a novel engine test configuration that removed uncertainty with regards to the effect of non-uniformity in the flow field on the kinetics. In real exhaust systems on passenger cars, packaging constraints determine the design of the exhaust and this is often non-ideal so that a mal-distributed flow field is supplied to the SCR catalyst. In a second set of experiments discussed in this paper the flow was supplied to the catalyst via a 180 ° diffuser. This gave a mal-distributed axially symmetric 3D flow field for experimental purposes, and therefore provided a test of the model's capability with non-uniform flow.

A CFD model has been developed based on kinetics that are available in the open literature. The kinetic scheme of Olsson et al. [1] has been used because it is a complete scheme, for a form of copper zeolite, and it is a simple scheme that uses

only one type of catalytic site. Other schemes are available, but some are for vanadium [2] or vanadium and an unspecified zeolite [3]. Some authors propose the existence of more than one type of site, for example Kamasamudram et al. [4], who propose sites that act as a reservoir for ammonia storage but then the ammonia must migrate to active sites before it can react. This complexity is avoided by the Olsson et al. [1] model.

Although the Olsson et al. scheme [1] supplies values for all the parameters and rate constants for their catalyst, it has been necessary to tune the kinetics for the catalyst used in the experiments here. In the experiments described in this paper, the engine exhaust was supplied to the SCR via a Pd DOC [5]. In this way exhaust NO_x comprised mainly of NO was supplied. Thus only the standard SCR reaction was playing a major role in the conversion. The 1D experiments were carried out specifically to enable tuning of the kinetic parameters for the standard reaction. The 3D experiments were then also carried out with a supply of mainly NO.

Changes have also been made to the ammonia adsorption and desorption kinetics as a result of the observations made in the 1D studies. Watling et al. [6] discuss the use of the well known expressions for ammonia adsorption and desorption, but indicate that these do not describe experimental observations. Some significant changes have been made here that do provide a much closer description of the experimental observations.

The tuned kinetic scheme for ammonia adsorption, desorption and standard SCR kinetics from the 1D studies has been applied to predictions for the 3D geometry that was studied experimentally. In that geometry, the exhaust flow passed through a 180° expansion prior to entering the SCR catalyst. These studies enabled the relative influence of local velocity and temperature to be assessed. This paper discusses the results and highlights the difficulties of using CFD simulations to predict NO_x conversion in a real engine exhaust system with non-ideal geometry.

ENGINE TESTING

The engine test rig is shown in [Figure 1](#). The experiments were carried out so that the exhaust stream from the engine passed through a Pd DOC placed downstream of a DPF. This non-standard configuration ensured that the DOC controlled the NO_x composition downstream and it was not influenced by soot on the DPF. The presence of a Pd DOC ensured that no HCs from the engine reached the SCR but that the NO from the engine via the DPF was not oxidised to NO₂ [5]. Thus the NO_x supplied to the SCR was mainly NO; the levels of NO₂ were observed to be negligible.

Downstream of the DPF and DOC the exhaust passes through a flow straightener placed in the smaller bore pipe just

upstream of the expansion box. The latter and the converging nozzle ensure that the flow at the nozzle exit is uniform. The long conical diffuser, with ten degree included angle, produced a uniform flow field that was applied to the SCR for tests that provided data for tuning the SCR kinetics. The SCR brick was 45 mm in length and 118.4 mm in diameter, of which 115 mm was exposed on the test rig. Its volume was approximately 0.5 litre. The cell density was 400 cpsi (62 cells/cm²) and the active catalyst was a form of copper zeolite.

The long conical diffuser could be replaced with a 180° sudden expansion, see [Figure 1](#), to supply non-uniform temperature and mal-distributed flow profiles to the SCR for a study of a 3D case. The flow profiles were axially symmetric. The concentration profiles as supplied to the SCR brick remained approximately uniform because the species were well mixed in the exhaust. A Horiba EXSA gas analyser monitored the NO_x from the engine. A Horiba FTIR 6000FT was used to measure the species concentrations upstream and downstream of the SCR. This had an uncertainty of 1% FSD for NO and was used on the 1000 ppm range; it had an uncertainty of 0.5% FSD for NH₃, again using the 1000 ppm range. The reductant supplied was 5% ammonia gas in nitrogen and this was injected at the point indicated in [Figure 1](#). The flow rate was controlled with a regulator valve and monitored with a calibrated flow-meter of the rotameter type. The 1D experiments carried out were transient experiments that were run to steady state conditions at three different ammonia dosing concentrations to evaluate the kinetics. Steady state experiments were performed when the 180° expander was used for the 3D studies.

KINETIC SCHEME AND MODIFICATIONS

Olsson et al. [1] describe a complete kinetic scheme for SCR over a type of copper zeolite, Cu-ZSM-5. This includes the standard, fast and slow SCR reactions and also N₂O formation, although not nitrate formation. Oxidation of NO and of NH₃ is also included. The scheme has the advantage of simplicity as only a single type of catalytic site is modelled. Olsson et al. provide values for kinetic rate parameters for all the reactions. These were deduced from their experimental observations and so are valid for their Cu-ZSM-5 zeolite. The catalyst used in the experiments here was a form of Cu β-zeolite and so tuning of the kinetics was necessary.

The standard reaction rate, mol/s/m³, from [1] was $[2.3E+08 \exp(-84900/RT)] C_{NO} \theta \Omega$.

This was changed to $[8.93E+05 \exp(-63484/RT)] C_{NO} \theta \Omega$.

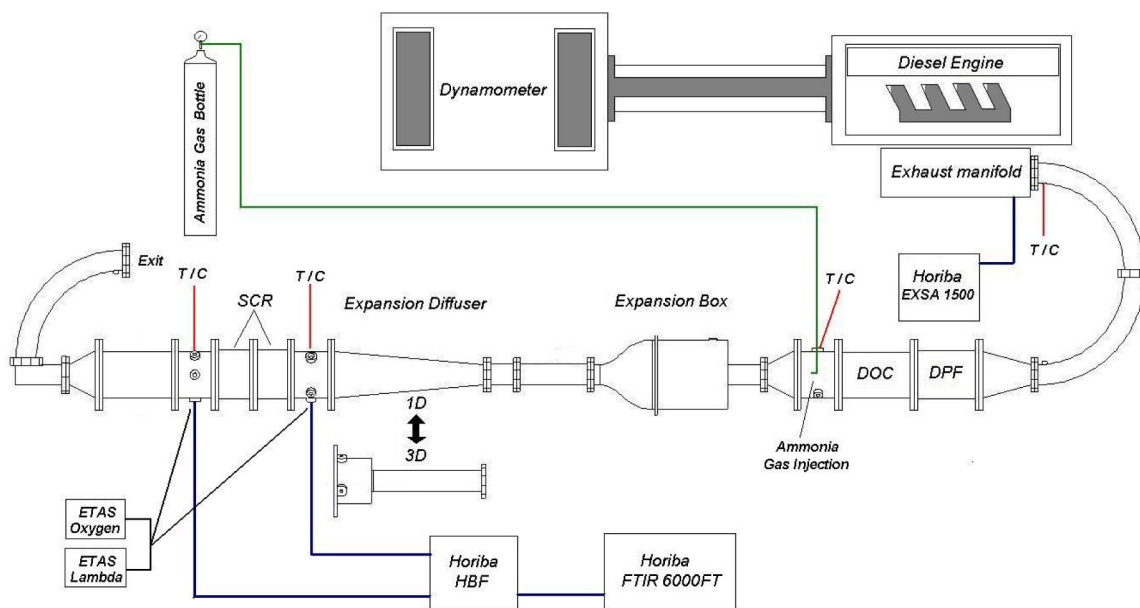


Figure 1. Schematic diagram of engine test rig and experimental SCR exhaust system. T/C indicates thermocouple location.

This rate was further modified by multiplying within a simulation by a local inhibition term $C_{NO}/(C_{NO} + C_{NO_2} + C_{NH_3})$.

This made an allowance for inhibition of the rate by competition between NO and ammonia for active sites on the catalyst. Inhibition by ammonia was observed in experiments here with a form of copper zeolite (Sturgess et al., [7]; Benjamin et al., [8]) and Olsson et al. [1] also indicate that there is inhibition by ammonia with Cu-ZSM-5 zeolite. Tronconi et al. [9] attempted to model inhibition by altering the form of the standard reaction rate expression but for a vanadium catalyst. Two recent papers, by Fedeyko et al. [10] and by Kamasamudram et al. [11], however, state clearly that although an inhibition effect is observed with Fe zeolite, it is not observed with Cu zeolite, which differs from observations here. In [11], however, it is conceded that the effect may occur on copper under conditions of very high ammonia concentration.

Furthermore, to match the kinetics to the experimental observations here, the ammonia adsorption and desorption expressions were adjusted to improve the description of net ammonia adsorption observed in experiments. It is necessary to distinguish between ammonia adsorption and ammonia storage. Ammonia must be adsorbed in order to be either stored or reacted; the ammonia storage rate can be written

$$\begin{aligned} \Omega \, d\theta/dt &= NH_3 \text{ adsorbed (net)} - NH_3 \text{ reacted} \\ &= NH_3 \text{ in} - NH_3 \text{ slip} - NH_3 \text{ reacted} \quad [\text{mol/s/m}^3] \end{aligned}$$

Thus the quantity $[NH_3 \text{ in} - NH_3 \text{ slip}]$ as observed in the engine tests can give a direct measure of the net ammonia adsorption rate for a brick of known size.

The adsorption rate, mol/s/m^3 , prescribed by Olsson et al. [1] is $[0.93 C_{NH_3} (1-\theta) \Omega]$.

This was changed to $[3.2 C_{NH_3} [\exp(-30)] \Omega]$.

The desorption rate, mol/s/m^3 , prescribed by Olsson et al. [1] is $[1.0 E+11 [\exp(-181500(1-0.98\theta)/RT)] \theta \Omega]$.

The term $(1-0.98\theta)$ makes the activation energy of desorption dependent upon θ , and a change was made so that it took the value $(1-0.2\theta)$ at low temperature or $(1-0.3\theta)$ at high temperature. In effect, this switched off desorption unless θ was very close to saturation. The capacity $\Omega \text{ mol sites/m}^3$ was given a temperature dependent value. The effect of these changes can be seen by comparing Figure 2 with Figure 3, and by comparing Figure 4 with Figure 5. The figures include the results of experiments where the supplied NO level was constant throughout, but the supplied ammonia level was initially in excess for the first 500 seconds of the test. This was turned down to a stoichiometric supply for about 300 s and then to a deficient supply for about 500 s. Finally, just before 1500 s, the ammonia supply was turned off. The NO and NH₃ levels downstream of the SCR were measured throughout. Figures 2, 3, 4, 5 show the plots of the species levels upstream and downstream of the SCR catalyst. The NH₃ out [data] and NO out [data] are the measured values downstream. The NO in and NH₃ in traces are from the simulation but they replicate the measured data. The NO out [CFD] and NH₃ out [CFD] traces are simulations from 1D CFD runs and the figures enable comparison of the data with the CFD predictions. Figures 2 and 4 show comparison of data traces with the simulation when using Olsson et al. kinetics at 270 °C and 210 °C respectively. Figures 3 and 5

show comparison of data traces with the simulation when using the revised kinetics at the high and low temperatures respectively. Excellent agreement between measurements and predictions can be seen in Figures 3 and 5 where the modified kinetic scheme was used.

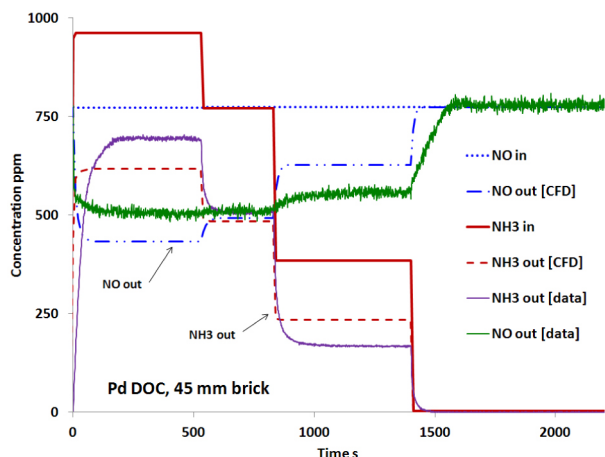


Figure 2. High temperature case, 270 °C, using parameter Ω 68 mol/m³ and Olsson kinetics parameter values.

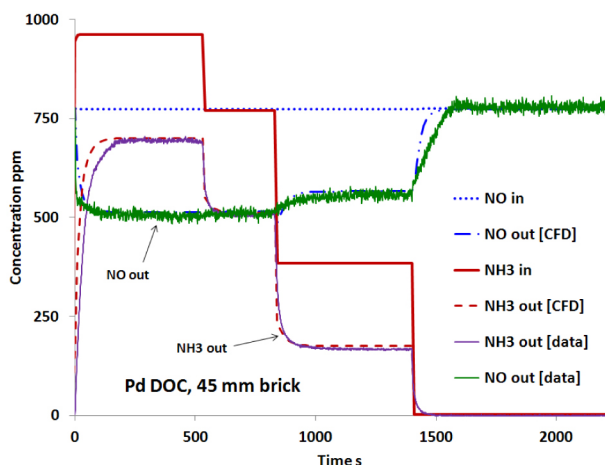


Figure 3. High temperature case, 270 °C, using parameter Ω 68 mol/m³ with modified kinetic parameters values.

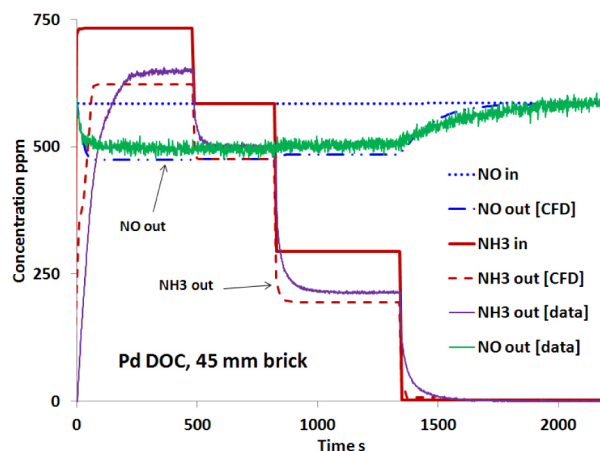


Figure 4. Low temperature case, 210 °C, using parameter Ω 90 mol/m³ with Olsson kinetics parameter values.

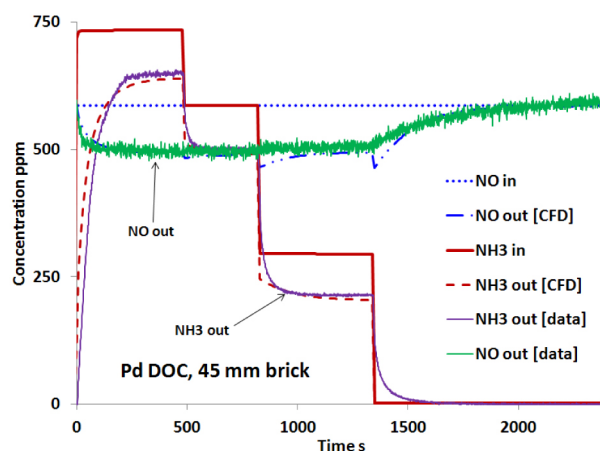


Figure 5. Low temperature case, 210 °C, using parameter Ω 90 mol/m³ with modified kinetic parameter values.

MEASUREMENTS WITH 3D GEOMETRY

The 180° expander replaced the long conical diffuser in the engine test rig, as indicated in Figure 1, and steady state measurements were carried out with a 45 mm length SCR brick. Profiles of temperature and concentration were measured in the exhaust system 20 mm upstream of the SCR brick and 30 mm downstream of the SCR brick. The velocity profile could not be measured on the engine test rig but was measured by placing the exhaust components on a laboratory air-flow rig and measuring the velocity profile with a hot wire anemometer traversing across the rear of the brick 30 mm from the exit.

CFD OF 3D STUDIES

The SCR catalyst brick was modelled by using the analogous porous medium approach, which is described in detail

elsewhere [12, 13]. The mesh used to model the 45 mm length SCR brick when supplied by a sudden expansion from the 50 mm diameter pipe is shown in Figure 6. The inlet boundary is 30 mm upstream of the sudden expansion. The small bore supply pipe at the inlet was modelled by 12 cells in the radial direction, the radius being 25 mm. There were 10 cells in the axial (flow) direction spanning 30 mm. The larger diameter of the expansion can, SCR brick and outlet pipe was 115 mm and the 57.5 mm radius was modelled with 28 cells radially. The expansion can was 100 mm in length and was spanned by 50 cells. The porous medium was 45 mm in length and was spanned by 15 cells. The outlet duct was 30 mm in length and was spanned by 10 cells. When the mesh is viewed in colour, the porous medium cells are light blue and the first row of porous medium cells is green so that it can be easily identified. The inlet duct is shown in red, the expansion can in orange and the exit duct in magenta. The mesh was the classic wedge shape with a 5 degree angle for 2D axially-symmetric simulations. The cell on the axis was slightly longer in the radial (x) direction, 3 mm, than the other cells, which were 2mm in length in the radial direction. Figure 7 shows the mesh used when modelling the brick only. In this mesh the expansion can has been removed and there are only 2 fluid cells upstream of the porous medium that represents the SCR brick. The inlet boundary is thus almost immediately upstream of the porous medium. Star-CD Version 4.14 modelled both the fluid and solid properties of the porous medium that represented the 45 mm length SCR monolith. The cells in the porous medium had length 3 mm in the axial (y) direction for the 45 mm brick. The cell sizes in the meshes were sufficiently small to provide a grid independent solution.

The pressure loss entrance effect in its simplest form [14] was applied in the simulations that used the mesh shown in Figure 6. The pressure loss was distributed across the porous medium such that

$$\Delta P/L = \alpha V^2 + \beta V$$

and where

$$\beta = \beta_0 + (0.5\rho U^2)/VL_{\text{substrate}}$$

The value for U was obtained for each x location from the row of cells immediately upstream of the porous medium and the correction was applied at the corresponding x location to all the porous medium cells. The mesh shown in Figure 7 was used for simulations where measured velocity and temperature profiles were applied to the inlet boundary. In these simulations the pressure loss was set to an artificially low value so that the velocity profile retained its shape and the flow was not subject to redistribution at the interface between the two layers of fluid cells downstream of the inlet boundary and the first layer of cells in the porous medium. The temperature profile applied was that measured at the exit from the porous medium. This also retained its shape in the

simulations because the outer walls were defined as adiabatic in this case. Thus the temperature and velocity profiles within the porous medium in the simulation were as close as possible to the real measured values. In the mesh shown in Figure 6, the outer wall was defined to be at a fixed temperature and the resistance to thermal loss was specified.

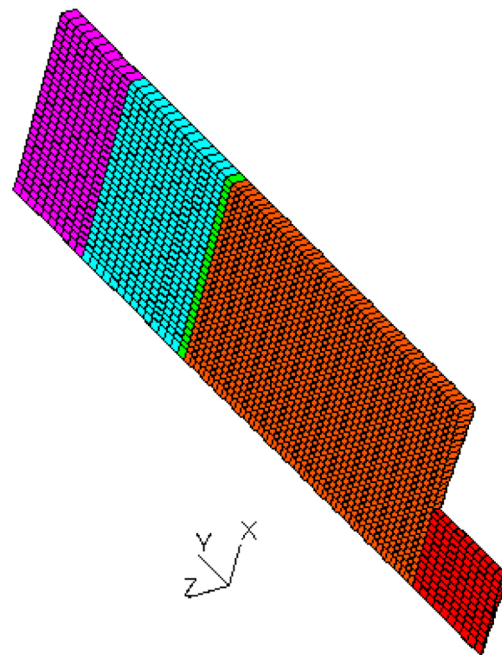


Figure 6. 2D axially-symmetric mesh for CFD simulation of sudden expansion.

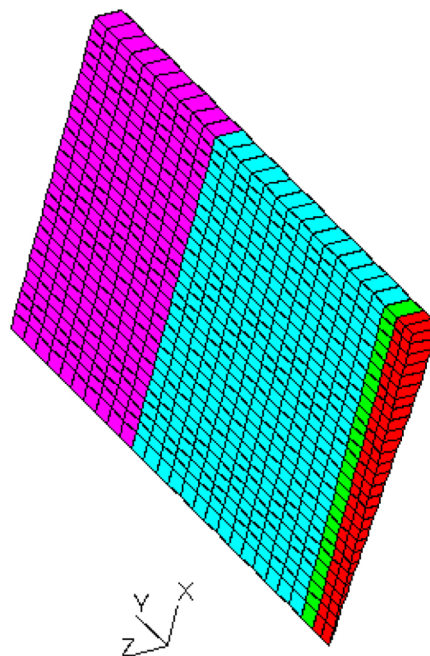


Figure 7. 2D axially-symmetric mesh for CFD simulation of SCR brick only.

The turbulence model used in the CFD simulations was the RNG k- ϵ model [15]. The MARS scheme, monotone advection and reconstruction scheme [16], was used as the differencing scheme but central differencing was used for both temperature and species concentration but blended with upwind differencing, blending factor 0.8. The Simple algorithm was used for the steady state simulations.

DISCUSSION OF RESULTS

Figure 8 shows measurements of species concentration profiles made in the expansion can 20 mm upstream of the SCR brick. This confirms that the exhaust and the ammonia reductant are well mixed and that concentration of both ammonia and NO is uniform despite the presence of large flow recirculation regions in the can. In Figure 8, the parameter 'a' is the ratio of supplied NH₃:supplied NO. Thus 0.5 corresponds to deficient ammonia, 1.0 to stoichiometric ammonia and 1.25 to excess ammonia. Table 1 lists the details of the species levels and the mass flow rate supplied in the experiment. These values were also used as the input data for the CFD simulations.

Table 1. Input data for CFD simulations

NO ppm (a=0.5)	541
NO ppm (a=1.0)	545
NO ppm (a=1.25)	553
NH ₃ ppm (a=0.5)	277
NH ₃ ppm (a=1.0)	553
NH ₃ ppm (a=1.25)	690
O ₂ %	9.3
MF g/s	26.6

Figure 9 shows the temperature profiles measured in the engine exhaust in the expansion can 20 mm upstream of the porous medium and also 30 mm downstream of the porous medium. The corresponding temperature values from the full CFD simulation using the mesh in Figure 6 are shown. In the can, the central flow jet has a higher temperature than the outer part of the flow field that extends out to the relatively cool can wall. Downstream of the porous medium, the temperature profile is very much flatter. In the can the flow redistributes in the distance between the measuring plane and the entrance to the porous medium. The passage of the flow through the porous medium may also tend to smooth and flatten the temperature profile as there is heat transfer from the flow to the porous medium and heat conduction within the solid phase of the porous medium. The exothermic effect of the SCR reactions is very small and this is not included in the model. The predicted downstream temperature profiles from the CFD model are warmer than the data suggest; upstream, the discrepancy is noticeable at the outer wall. Presumably the heat loss from the can is slightly greater in the real exhaust system than the allowance that is made in the model.

The velocity profile in the porous medium was investigated by putting the 180° sudden expansion on a cold flow rig and measuring the velocity profile downstream of the SCR brick with a hot wire anemometer. Figure 10 shows the CFD predictions: for the measurement plane in the can 20 mm upstream of the porous medium, for the row of cells immediately upstream of the porous medium and for the measurement plane 30 mm downstream of the porous medium. The profile 20 mm upstream of the brick (Y 111 mm) shows the presence of the jet in the centre with diameter just less than 50 mm and negative velocity components are seen at the periphery because of the presence of large recirculating vortices in the expansion can. The profiles immediately upstream and 30 mm downstream of the SCR brick are more similar with the downstream profile showing slightly higher velocity on the periphery at radius 0.057 m. This higher velocity together with cool temperatures at the periphery would be expected to cause breakthrough of unconverted NO and NH₃ and consequent low conversion efficiency at the periphery. This is discussed further below.

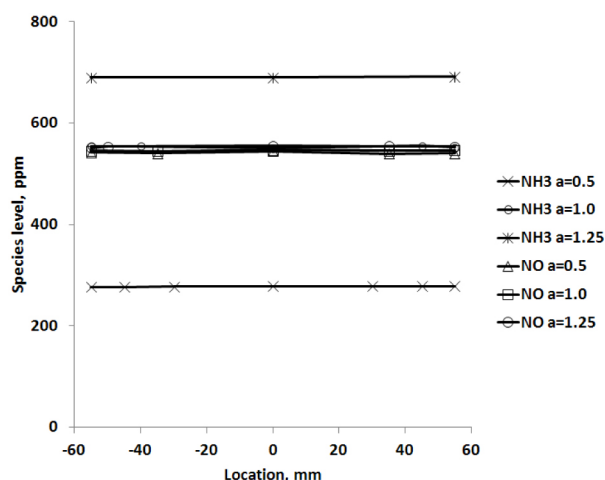


Figure 8. Measured concentration profiles 20 mm upstream (Y 111 mm) of 45 mm SCR brick in the expansion can. Measurements for deficient ammonia (a=0.5), stoichiometric ammonia (a=1.0) and excess ammonia (a=1.25).

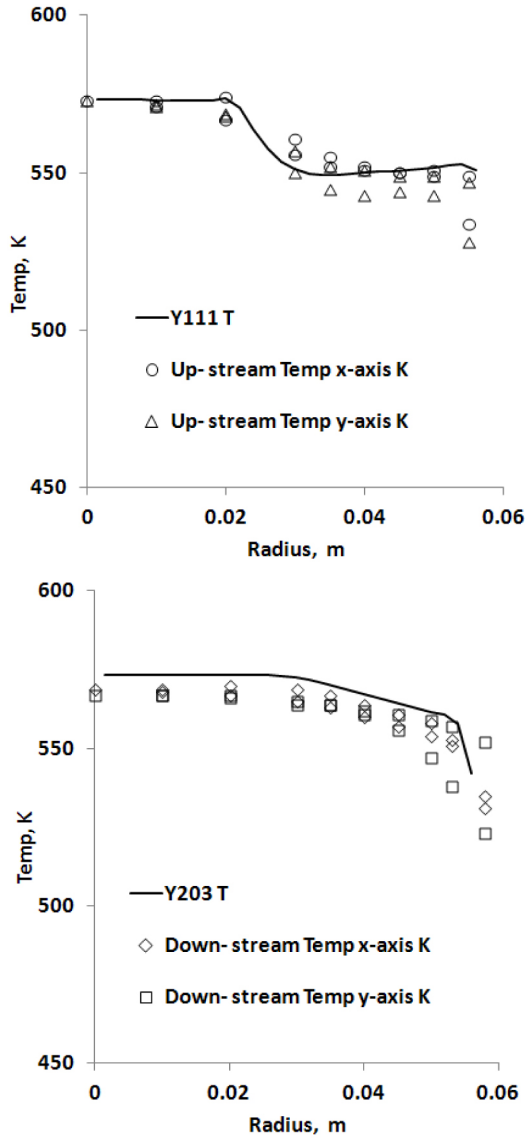


Figure 9. Temperature profiles 20 mm upstream (Y 111 mm) and 30 mm downstream (Y 203 mm) of 45 mm SCR brick; lines are from CFD simulation; symbols are data. Horizontal and vertical traverses are indicated by x-axis and y-axis.

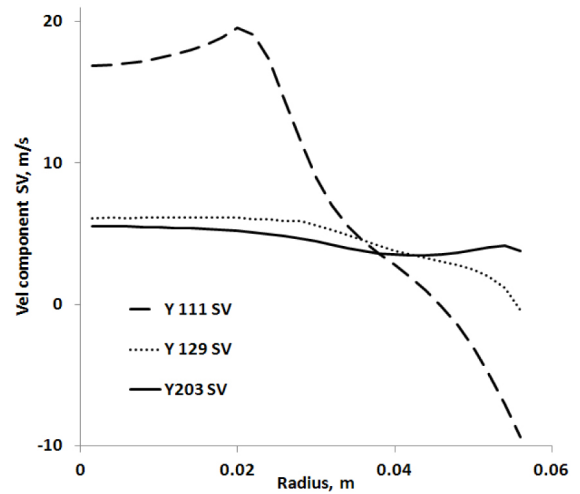


Figure 10. Velocity profiles of V component from full CFD simulation. Profiles are shown for 45 mm SCR brick about 20 mm upstream of brick (Y 111 mm), immediately upstream of brick (Y 129 mm) and 30 mm downstream of brick (Y 203 mm).

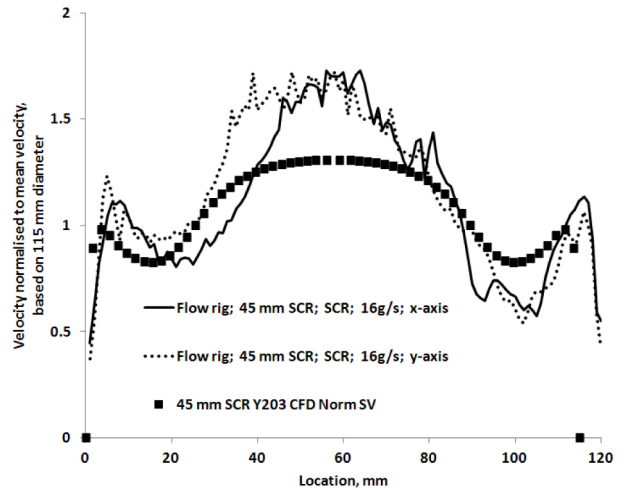


Figure 11. Comparison of normalised exit velocity measured on a flow rig with normalised exit velocity predicted by the CFD simulation for the 45 mm length SCR brick placed downstream of the sudden expansion. Horizontal and vertical traverses are indicated by x-axis and y-axis.

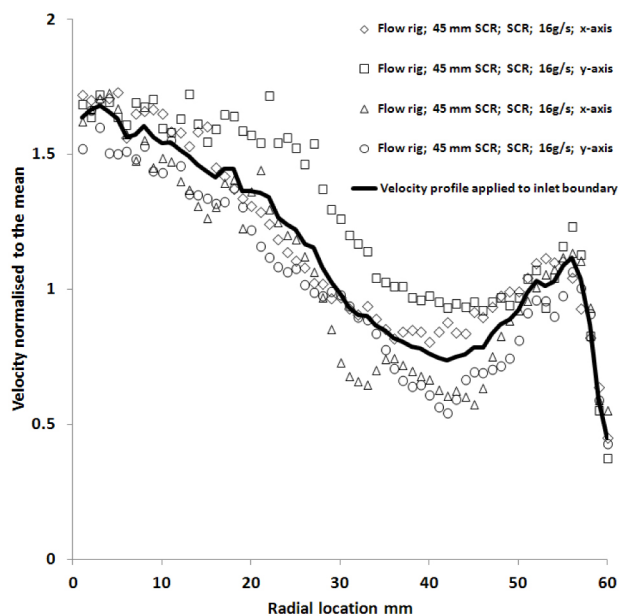


Figure 12. Normalised velocity measured on a flow rig. Horizontal and vertical traverses are indicated by x-axis and y-axis. The velocity profile applied to the inlet boundary of the mesh shown in Figure 7 is indicated.

Figure 11 shows the comparison between the normalized velocity measured at the exit from the SCR brick when placed downstream of the sudden expansion on a cold flow rig and when predicted by CFD simulation for hot flow conditions that prevail in the engine tests. The mass flow rate in the engine tests that took place near 300 °C was 26.6 g/s. For tests on the cold flow rig, at temperature 19.3 °C, the flow rate was set at 16 g/s so that the tests on the flow rig were carried out at approximately the same Reynolds number as the high temperature engine tests. The measurements for the 45 mm brick, Figure 11, made with hot wire anemometry on a flow rig are not smooth even though they were made within a 120 mm diameter sleeve and 30 mm from the brick exit. Nevertheless, the overall agreement with the CFD predictions obtained by including the pressure loss entrance effect appears fairly good at the periphery although the agreement is poorer on the axis, at location 57.5 mm in Figure 11. Figure 12 shows the average profile of the velocity normalized to the mean based on the measurements in Figure 11. This velocity profile can be applied to the inlet boundary when running the CFD model using the mesh shown in Figure 7.

Figure 13 shows the measured NO and ammonia conversion data from the engine tests compared with CFD predictions from the full simulation model. The data are discussed first. Low conversion rates are seen at the periphery, i.e. at radius greater than 55 mm, as a consequence of the low temperature (Figure 9) and fairly high velocity (Figure 12) in this region. The velocity profile exhibits its primary peak on the axis but also a significant secondary peak at radius 55 mm, see Figure 12. There is a velocity minimum at radius 40 mm. Thus the

residence time is lower at radius 55 mm than at radius 40 mm. The results indicate that cooling at the wall together with the lower residence time in that region has decreased reaction rates in that region. The highest observed conversion rates are at radius 40 mm where the velocity is lowest and hence the residence time is greatest. On the axis, temperature is high but velocity is also high so residence time is low and in consequence conversion is low.

The CFD prediction from the full model for the stoichiometric case ($a=1.0$) in Figure 13 describes the data fairly well. In the case where ammonia is deficient ($a=0.5$), however, there is under-prediction of conversion of NO on the axis and towards the periphery, and under-prediction of conversion of ammonia most notably on the axis. In the case where the ammonia supply was in excess ($a=1.25$), the predicted ammonia conversion profile matches the data quite well. The conversion of NO is under-predicted in this case, most notably on the axis. Although the CFD predicted temperature is slightly too high at the periphery, see Figure 9, and the predicted secondary velocity peak is slightly too low, see Figure 11, overall there is fair agreement between the data and predictions at the periphery.

In order to investigate the relative importance of the influence of temperature and velocity on the predictions, the CFD model was run using the mesh in Figure 7 with the measured temperature profile supplied to the inlet boundary but the velocity set as uniform and equal to the mean velocity. The results are shown in Figure 14. Agreement is very good on the axis in every case but the profile shapes are not consistent with the observations. It is clear that the fall-off of temperature at the periphery is not the parameter that is controlling the observed profile shapes. Figure 15 shows the results from simulations using the mesh in Figure 7 where the measured temperature profile was supplied to the inlet boundary and where the measured velocity profile, Figure 12, was also supplied.

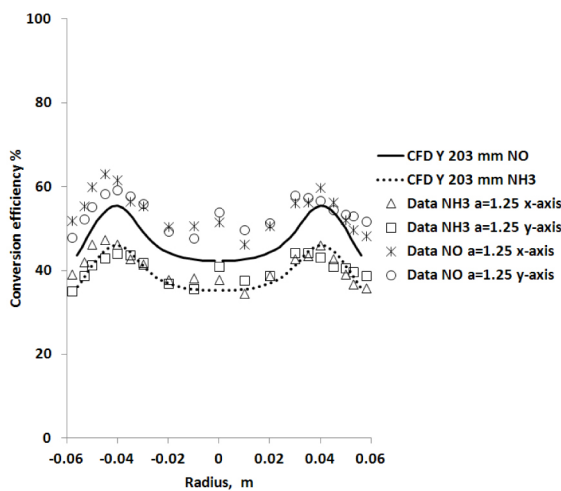
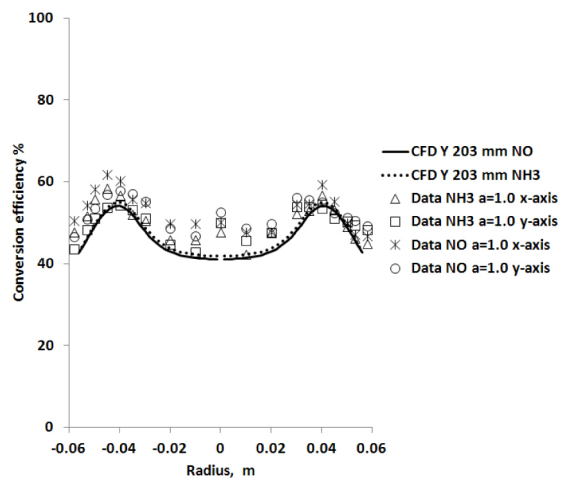
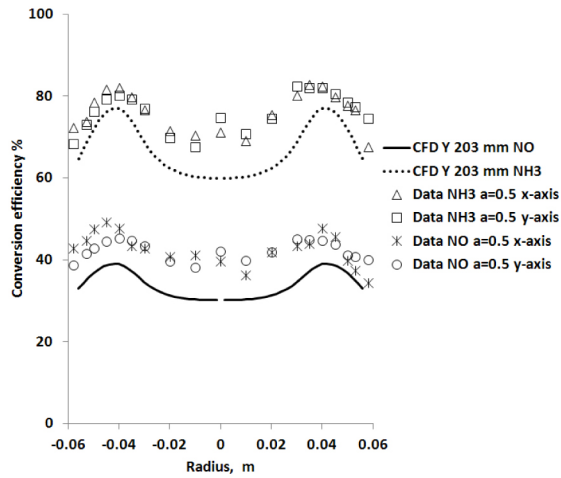


Figure 13. Conversion profiles for deficient ammonia (*a* 0.5), stoichiometric (*a* 1.0) and excess ammonia (*a* 1.25) cases 30 mm downstream (*Y* 203mm) of 45 mm SCR brick; lines are from full CFD simulation; symbols are data. Horizontal and vertical traverses are indicated by *x*-axis and *y*-axis.

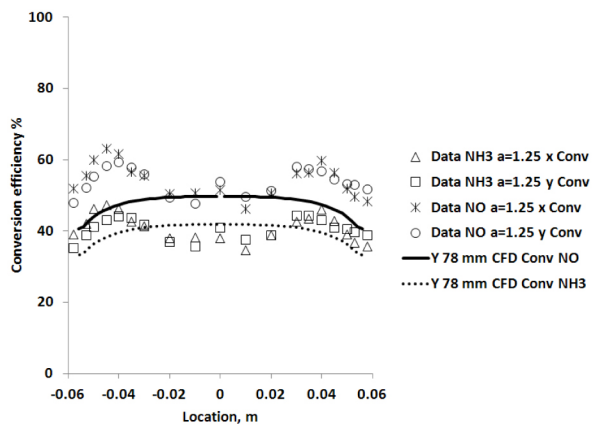
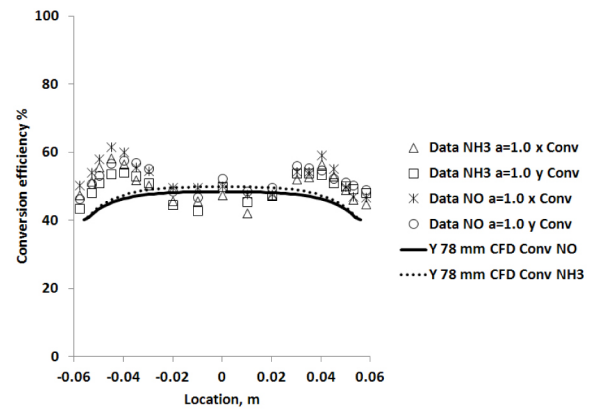
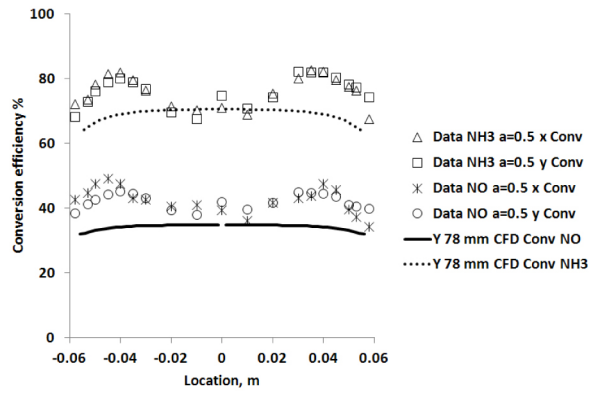


Figure 14. Conversion profiles for deficient ammonia (*a* 0.5), stoichiometric (*a* 1.0) and excess ammonia (*a* 1.25) cases 30 mm downstream (*Y* 78mm) of 45 mm SCR brick; lines are from CFD simulation of brick only applying observed temperature profile and mean velocity; symbols are data. Horizontal and vertical traverses are indicated by *x*-axis and *y*-axis.

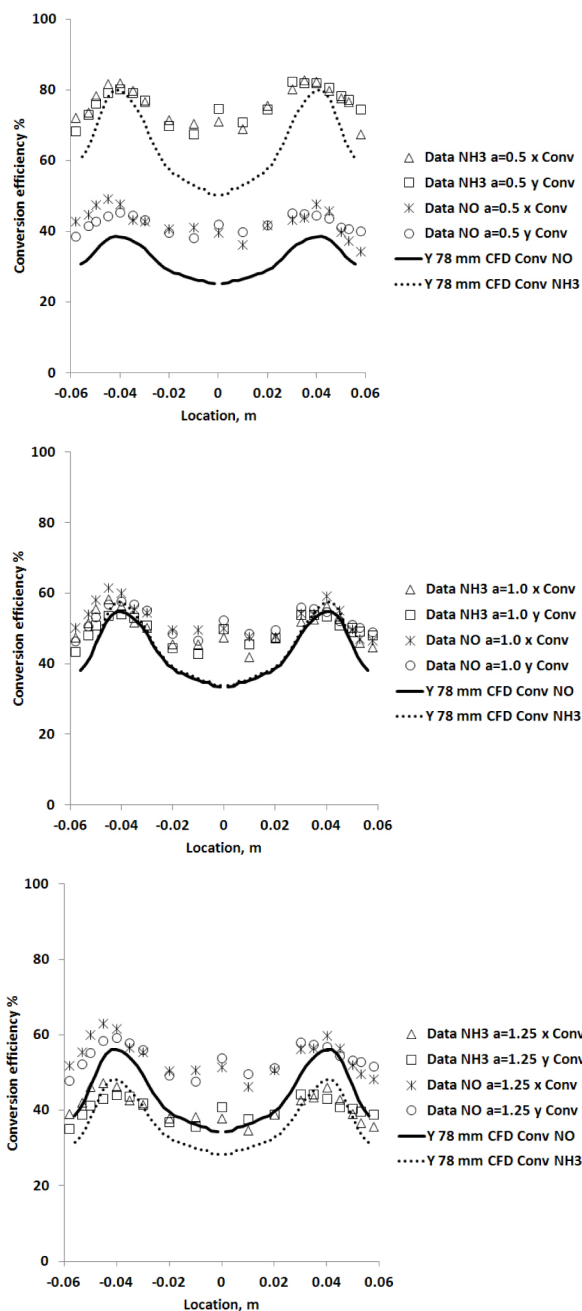


Figure 15. Conversion profiles for deficient ammonia (a 0.5), stoichiometric (a 1.0) and excess ammonia (a 1.25) cases 30 mm downstream (Y 78mm) of 45 mm SCR brick; lines are from CFD simulation of brick only applying observed temperature profile and observed velocity profile; symbols are data. Horizontal and vertical traverses are indicated by x-axis and y-axis.

The outcome, as seen in Figure 15, is CFD-predicted profiles that match the observations more closely. There are discrepancies in conversion values, notably on the axis for deficient, stoichiometric and excess ammonia but it is clear that the observed profile shapes are the consequence of both the temperature and velocity profiles in the SCR brick.

This implies that the prediction of velocity profile in a CFD model remains vitally important in understanding the conversion that occurs in the catalyst brick. Although the simple pressure loss entrance effect correction does provide an improved velocity prediction, this may not be good enough for accurate prediction of conversion in a more complex 3D flow field.

SUMMARY/CONCLUSIONS

In this paper the kinetics for the standard SCR reaction were modified to give very good CFD predictions of the conversion of NO at temperatures between 200 and 300 °C on a form of copper zeolite. Some experiments were performed with the SCR brick downstream of a 180 degree expansion. Measurements upstream of the brick showed non-uniform temperature profiles in the expansion can but uniform concentration profiles. Conversion of NO and ammonia in the 45 mm SCR brick gave non-uniform distributions of these species downstream of the brick. CFD simulations based on a 2D-axisymmetric model were able to match the experimental profiles. It was demonstrated that both temperature and velocity influence conversion. Accurate predictions of the velocity and temperature profiles within the brick are important for achieving good predictions of conversion efficiency.

REFERENCES

1. Olsson, L., Sjoval, H., Blint, R. J.. A kinetic model for ammonia selective catalytic reduction over Cu-ZSM-5. Applied catalysis B: Environmental. Vol. 81 (2008) pp 203-217
2. Chi, J. and DaCosta, H., "Modeling and Control of a Urea-SCR Aftertreatment System," SAE Technical Paper 2005-01-0966, 2005, doi:10.4271/2005-01-0966.
3. Chatterjee, D., Burkhardt, T., Weibel, M., Nova, I. et al., "Numerical Simulation of Zeolite- and V-Based SCR Catalytic Converters," SAE Technical Paper 2007-01-1136, 2007, doi:10.4271/2007-01-1136.
4. Kamasamudram, K., Currier, N. W., Chen, X., Yezerets, A.. Overview of the practically important behaviors of zeolite based urea-SCR catalysts, using compact experimental protocol. Catalysis Today. Vol. 151 (2010) pp 212-222
5. Salasc, S., Skoglundh, M. and Fridell, E.. A comparison between Pt and Pd in NOx storage catalysts. Applied Catalysis B: Environmental. Vol. 36 (2002) 145-160
6. Watling, T., Tutuianu, M., Desai, M., Dai, J. et al., "Development and Validation of a Cu-Zeolite SCR Catalyst Model," SAE Technical Paper 2011-01-1299, 2011, doi: 10.4271/2011-01-1299.
7. Sturgess, M., Benjamin, S., and Roberts, C., "Spatial Conversion Profiles within an SCR in a Test Exhaust System with Injection of Ammonia Gas Modelled in CFD using the

Porous Medium Approach,” SAE Technical Paper 2010-01-2089, 2010, doi:[10.4271/2010-01-2089](https://doi.org/10.4271/2010-01-2089).

8. Benjamin, S. F., Gall, M., Sturgess, M. P., Roberts, C. A.. Experiments on a light duty SCR test exhaust system using ammonia gas to provide data for validation of a CFD model. Proceedings of I Mech E Conference Internal Combustion Engines: Improving Performance, Fuel Economy and Emissions, London, November 2011
9. Tronconi, E., Nova, I., Ciardelli, C., Chatterjee, D., Bandl-Konrad, B., Burkhardt, T.. Modelling of an SCR catalytic converter for Diesel exhaust after treatment: Dynamic effects at low temperature. *Catalysis Today*. Vol. 105 (2005) pp 529-536
10. Fedeyko, J. M., Chen, B., Chen, H-Y. Mechanistic study of the low temperature activity of transition metal exchanged zeolite SCR catalysts. *Catalysis Today*. Vol. 151 (2010) pp 231-236
11. Kamasamudram, K., Currier, N., Szailer, T., and Yezerets, A., “Why Cu- and Fe-Zeolite SCR Catalysts Behave Differently At Low Temperatures,” *SAE Int. J. Fuels Lubr.* 3(1):664-672, 2010, doi:[10.4271/2010-01-1182](https://doi.org/10.4271/2010-01-1182).
12. Benjamin, S. F., Roberts, C. A., Three-dimensional modelling of NO_x and particulate traps using CFD: A porous medium approach. *Applied Mathematical Modelling*. Vol. 31 (2007) 2446-2460
13. Benjamin, S. F., Roberts, C. A.. The porous medium approach applied to CFD modelling of SCR in an automotive exhaust with injection of urea droplets. Proceedings of IMechE Internal Combustion Engines: Performance, Fuel Economy and Emissions, London, December 2007
14. Quadri, S. S., Benjamin, S. F., Roberts, C. A.. An experimental investigation of oblique entry pressure losses in automotive catalytic converters. *Proc I Mech E Part C: J Mech Eng Sci*. Vol. 223 (2009) 2561-2569
15. Yakhot, V., Orszag, S. A., Thangam, S., Gatski, T. B., Speziale, C. G.. Development of turbulence models for shear flows by a double expansion technique. *Physics of Fluids*. Vol. A4(7) (1992) 1510-1520
16. CD-adapco. Methodology Manual for Star-CD software, Version 4.14

CONTACT INFORMATION

s.benjamin@coventry.ac.uk

ACKNOWLEDGMENTS

This work was carried out with technical support from Jaguar-LandRover, Faurecia and Johnson Matthey, which is gratefully acknowledged. The hot wire anemometry measurements were carried out at Coventry University by Piotr Skusiewicz. Robert Gartside of Coventry University provided technical assistance. Funding was supplied by EPSRC, UK (Grant No. EP/FO36175/1).

DEFINITIONS/ABBREVIATIONS

- a** - Ratio of ammonia to NO_x
- C_{NO}** - NO concentration
- C_{NO2}** - NO₂ concentration
- C_{NH3}** - NH₃ concentration
- L** - Length
- ΔP** - Pressure loss
- R** - Gas constant
- T** - Temperature
- t** - Time
- U** - Transverse velocity component
- V** - Axial velocity component
- α** - Permeability coefficient
- β** - Permeability coefficient
- ρ** - Density
- θ** - Fraction of sites occupied
- Ω** - Capacity, mol-sites/m³

The Engineering Meetings Board has approved this paper for publication. It has successfully completed SAE's peer review process under the supervision of the session organizer. This process requires a minimum of three (3) reviews by industry experts.

All rights reserved. No part of this publication may be reproduced, stored in a retrieval system, or transmitted, in any form or by any means, electronic, mechanical, photocopying, recording, or otherwise, without the prior written permission of SAE.

ISSN 0148-7191

Positions and opinions advanced in this paper are those of the author(s) and not necessarily those of SAE. The author is solely responsible for the content of the paper.

SAE Customer Service:

Tel: 877-606-7323 (inside USA and Canada)

Tel: 724-776-4970 (outside USA)

Fax: 724-776-0790

Email: CustomerService@sae.org

SAE Web Address: <http://www.sae.org>

Printed in USA